Available online at www.sciencedirect.com
SCIENCE DIRECT®
International Journal of Heat and Mass Transfer 49 (2006) 2652–2662
International Journal of HEAT and MASS TRANSFER
www.elsevier.com/locate/ijhmt

Investigation of mixed convection heat transfer in a horizontal channel with discrete heat sources at the top and at the bottom

A. Dogan [a], M. Sivrioglu [b], S. Baskaya [b,*]

[a] Department of Mechanical Engineering, Cumhuriyet University, 58140 Kampus, Sivas, Turkey
[b] Faculty of Engineering and Architecture, Department of Mechanical Engineering, Gazi University, 06570 Maltepe, Ankara, Turkey

Received 20 May 2005; received in revised form 20 December 2005
Available online 6 March 2006

Abstract

Mixed convection heat transfer from arrays of discrete heat sources inside a horizontal channel has been investigated experimentally. Each of the lower and upper surfaces of the channel was equipped with 8×4 flush mounted heat sources subjected to uniform heat flux. Sidewalls, lower and upper walls are insulated and adiabatic. The experimental parametric study was made for aspect ratios of AR = 2, 4 and 10, at various Reynolds and Grashof numbers. From the experimental measurements, row-average surface temperature and Nusselt number distributions of the discrete heat sources were obtained and effects of Reynolds and Grashof numbers on these numbers were investigated. From these results, the buoyancy affected secondary flow and the onset of instability have been discussed. Results show that top and bottom heater surface temperatures increase with increasing Grashof number. The top heater average-surface temperatures for AR = 2 are greater than those of bottom ones. For high values of Grashof numbers where natural convection is the dominant heat transfer regime ($Gr^*/Re^2 \gg 1$), temperatures of top heaters can have much greater values. The variation of the row-average Nusselt numbers for the aspect ratio of AR = 4, show that with the increase in the buoyancy affected secondary flow and the onset of instability, values of Nusselt number level off and even rise as a result of heat transfer enhancement especially for low Reynolds numbers.

Keywords: Mixed convection; Discrete heat sources; Channel flow; Electronic cooling

1. Introduction

Mixed convection cooling is applied in a wide range of engineering applications like heat exchangers, electronic equipment and similar industrial applications. Especially, heat transfer from continuously heated surfaces, in relation to cooling of electronic equipment, has become a subject of interest in the last decade, because of advances in integrated circuit technology. Microminiaturization of electronic components for digital computers has resulted in increased circuit densities with large power dissipation rates per unit area of the components. The researchers of electronic cooling therefore have had increased interest in the analysis of fluid flow and heat transfer in discrete heating situations.

The common methods used for the cooling of electronic equipment include free and forced convection using air or liquid as the coolant. Air cooling has been the most popular method due to the simplicity it affords in cooling design.

The study of one discrete heat source between horizontal parallel planes under mixed convection conditions by Kennedy and Zebib [1] is among earlier investigations on electronic cooling. In this study four different local heat source configurations were studied numerically and experimentally. Another of these earlier studies was conducted by Incropera et al. [2] who had investigated heat transfer from a single and an array of flush mounted heat sources for water and FC-77 in a rectangular channel. Incropera presented an extensive review and discussion of work done on the convective heat transfer in electronic equipment

* Corresponding author. Tel.: +90 312 2317400x2421; fax: +90 312 2308434.
E-mail address: baskaya@gazi.edu.tr (S. Baskaya).

0017-9310/$ - see front matter © 2006 Elsevier Ltd. All rights reserved.
doi:10.1016/j.ijheatmasstransfer.2006.01.005

Nomenclature

A_c	channel cross-sectional area, m^2
A_s	heat source surface area, m^2
AR	dimensionless aspect ratio, W/H
c_p	specific heat, kJ/kg K
D_h	channel hydraulic diameter, $4A_c/P$, m
F	dimensionless radiation view factor
g	gravitational acceleration, m/s^2
$Gr^*_{D_h}$	dimensionless modified Grashof number, $Gr^*_{D_h} = (g\beta\bar{q}_c D_h^4)/(k_{air}\nu_{air}^2)$
H	channel height, m
k	thermal conductivity, W/mK
$\overline{Nu}_j$	dimensionless row-average Nusselt number, $\overline{Nu}_j = (Q_{c_j} D_h)/(A_{s_j}(\overline{T}_{s_j} - T_b)k_{air})$
P	perimeter, m
Pr	Prandtl number, $Pr = c_{p_{air}}\mu_{air}/k_{air}$
$\bar{q}_c$	average convection heat flux, W/m^2
Q_c	convection heat transfer rate, W
Q_{cond}	conduction heat transfer rate, W
Q_{rad}	radiation heat transfer rate, W
Q_{tot}	total power dissipation, W
R	electrical resistance, Ω
$Ra^*_{D_h}$	modified Rayleigh number, $Ra^*_{D_h} = Gr^*_{D_h}Pr$
Re_{D_h}	Reynolds number, $Re_{D_h} = (U_{in}D_h)/\nu_{air}$
Ri	Richardson number, $Ri = Gr^*_{D_h}/Re^2_{D_h}$
T	temperature, °C
$\overline{T}_b$	bulk mean temperature, °C
$\overline{T}_j$	row-average temperature, °C
U_{in}	mean longitudinal velocity, m/s
V	voltage, V
W	channel width, m

Greek symbols

β	thermal expansion coefficient, 1/K
ε	heater surface emissivity
μ	dynamic viscosity, kg/ms
ν	kinematic viscosity, m^2/s
σ	Stefan–Boltzmann constant, $W/m^2\,K^4$

Subscripts

air	air
b	bulk fluid quantity
bottom	bottom
i	heater column index ($i = 1,2,3,4$)
j	heater row index ($j = 1,2,3,\ldots,8$)
o	inlet
s	heat source surface
top	top

cooling, summarizing various convection cooling options. A review of the channel flow problem applied to electronic cooling was also presented by Peterson and Ortega [3]. A great number of analytical, numerical and experimental works has been carried out on similar problems since these earlier investigations. A large variety of fluids were used in these studies. Heindel et al. [4] presented numerical predictions and experimental data for natural convection from discrete heat sources flush mounted on one vertical wall of a vertical cavity for water and FC-77. Choi and Cho [5] examined the effect of the aspect ratio of rectangular channels with discrete heat sources on the cooling performance of paraffin slurry. Most of the studies in the literature however, are regarding vertical channels. Natural, forced and mixed convection heat transfer from protruding and flush-mounted discrete heat sources inside vertical channels have been investigated by McEntire and Webb [6], Grimella and Eibeck [7], Turkoglu and Yucel [8], Fuji et al. [9], Tso et al. [10] and Tsay [11] for air and water. An inclined channel was used by Yucel et al. [12] in their numerical study of mixed convection from isothermally heated discrete heat sources. Choi and Ortega [13] studied numerically the mixed convection in an inclined channel with discrete heat sources subjected to uniform heat flux.

The following investigations are regarding horizontal channel configurations. Heat transfer from a horizontal printed circuit board under fully developed laminar mixed convection flow conditions was investigated by Leung et al. [14] and Leung and Kang [15] experimentally and numerically. The circuit board was represented by a plate with rectangular ribs mounted orthogonal to the mean air-flow. Experiments and numerical computations were performed by Mahaney et al. [16] on heat transfer from flush mounted discrete heat sources in a horizontal rectangular channel for water. Heat transfer regimes characterized by pure natural convection, mixed convection, laminar forced convection, and the initiations of transition to turbulence were investigated.

As can be observed from the above presentation most studies are for vertical channels with protruding heat sources with water as the heat transfer fluid. Only few investigations can be found in the literature regarding the heat transfer from discrete heat sources inside horizontal channels for air. Hacohen et al. [17] made one of these studies. Their investigation comprised an experimental and theoretical study for both forced and free convection with both flush-mounted and protruding heat sources. Effects of channel geometry, component array height, air-flow rate and heat flux were studied. From measurements and calculations they argue that the heat transfer coefficient for each individual element falls between two limiting theoretical values. An experimental conjugate heat transfer investigation on discrete heat sources flush-mounted on a conductive substrate in a horizontal channel for air was performed by Hwang [18]. However, this study was for forced convection conditions. Effects of free-stream turbulence, free-stream

velocity and substrate conductivity were investigated. They showed that substrates of higher conductivity can spread more source heat by board conduction and smooth off local heat transfer coefficient distributions. In addition, they argue that free-stream turbulence can enhance the heat transfer. Finally, for the first time, correlations of source-averaged Nusselt numbers for various free-stream turbulence intensities are presented in terms of the Reynolds number and the substrate-to-fluid conductivity ratio. Mahaney et al. [19] numerically studied three-dimensional mixed convection heat transfer from an array of discrete heat sources in a horizontal rectangular duct. Numerical results showed that the variation of the row-average Nusselt number with Reynolds number exhibits a minimum, suggesting that heat transfer may be enhanced due to buoyancy-induced secondary flow by reducing the flow rate and hence the pumping requirements.

From the above literature review, one can see that only little information can be found in literature for mixed convection heat transfer from flush mounted discrete heat sources in horizontal channels when the working fluid is air and in almost all these studies, heat sources were placed at only one wall of the channel considered. The present research will try to fill this gap to some extent. This study is a continuation of studies performed by the second and last author on mixed convection heat transfer in channel flows as presented by Ozsunar et al. [20,21]. Some initial results from the present study can be found in Dogan et al. [22].

2. Experimental set-up and data reduction

Information on the experimental apparatus, devices used and procedures followed are given in detail by Dogan [23]. A summary of that information is presented below.

2.1. Experimental set-up

Fig. 1. shows a schematic representation of the experimental set-up. The nozzle section, test section and the whole channel are fixed on a metal framework for rigidity purposes. A blower is used to draw air through the whole channel assembly. The flow rate is measured with a hot-wire-anemometer (Testovent 4200) with an accuracy of $\pm 1.5\%$. A control valve was used to control the flow rate. The test section is isolated from the blower acoustically and mechanically with a damping chamber and flexible hosing. At the channel entrance a nozzle with flow straighteners has been used in order to suppress turbulence and achieve steady, laminar flow conditions with a uniform velocity distribution. The flow straightener was made of 5-mm diameter and 50-mm long plastic hoses. In addition, a filter is used to filter the incoming air. The nozzle is made of 0.5-mm thick aluminum sheet with a contraction ratio of 20:1, and has been designed to eliminate flow separation, minimize turbulence, and provide a uniform velocity profile at the channel entrance.

The test section is a rectangular duct heated both at the top and the bottom with a cross-section of 200-mm in width. The height of the cross-section was adjusted during the experiments, so that it provides an aspect ratio which can be selected among AR = 2, 4 and 10. The total length of the duct is 1500-mm, comprising 850-mm entry and 150-mm exit regions with a 500-mm test section in between. The 850-mm unheated entrance region before the test section was used to achieve hydrodynamic boundary layer thicknesses which were greater than or close to the half of the channel height at the inlet of the test section. The top, sides and bottom entry and exit regions of the duct are constructed of 5-mm thick plexi-glass. The sides of the channel

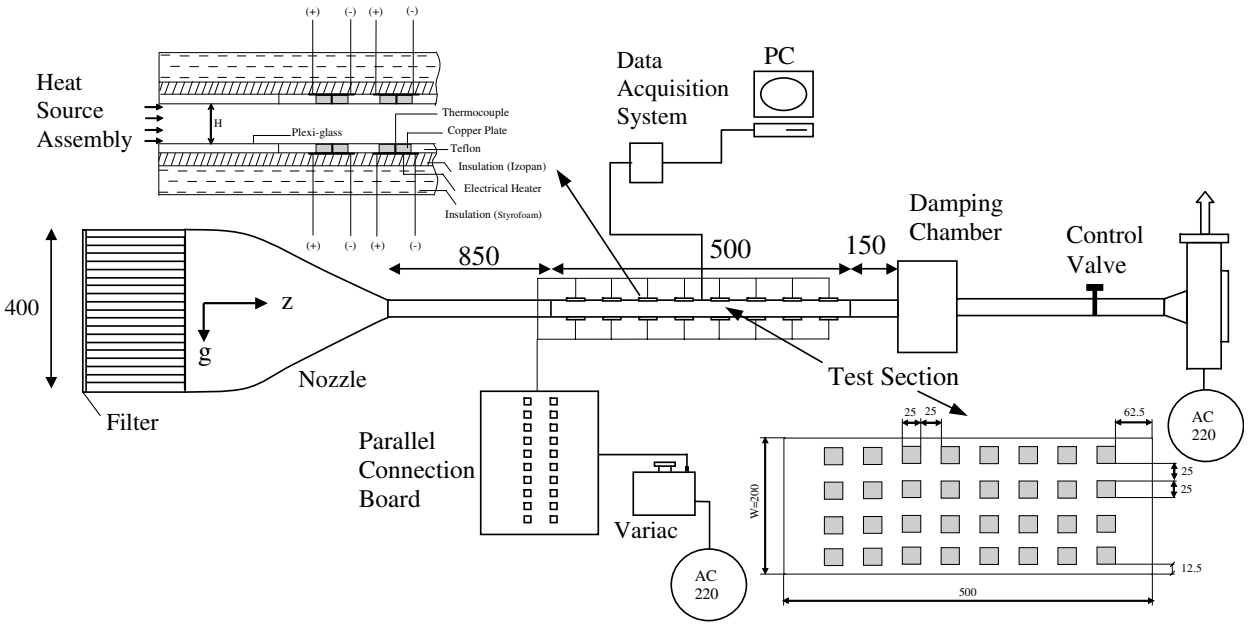

Fig. 1. Schematic diagram of the experimental set-up, heat source layout and assembly (measures are in mm).

were insulated with 50-mm Styrofoam. The top and the bottom walls of the test section are made of 5-mm thick pure teflon (PTFE) ($k = 0.25$ W/mK) in which the heat sources are embedded. This heated section was insulated with 20-mm Glasswool (Izopan) and 50-mm Styrofoam. Distributions of discrete heat sources in the test section were the same for both the top and bottom walls and their layout is also shown in Fig. 1 with all the necessary dimensions. Eight rows were used in the flow direction consisting of four heat sources in each row of top and bottom walls giving a total of 64 heat sources. Heater dimensions were 25×25 mm. The heater sections of the teflon substrate were cut using an industrial laser.

The construction of the discrete heat sources is schematically shown as an inset in Fig. 1. As can be seen from this figure, copper blocks ($k = 386$ W/mK, $\varepsilon = 0.3$) used were tightly fit to the top and the bottom teflon substrate. The area of resistance wire heating element was the same as that of copper block. The heating elements were electrically insulated and the resulting assembly was screwed to the copper blocks using a heat sink compound providing the least possible contact resistance. The heater blocks were equipped with 24-gauge copper–constantan thermocouples one for each and at the centre of the block. Electric current was provided to the heaters via a variac and a parallel connection board. Power dissipation was determined by measuring the voltage drop and resistance across the heater blocks and by making use of the total surface area values of the heaters. A Goldstar multimeter with accuracy of $\pm 0.5\%$ for voltage and $\pm 0.2\%$ for resistance was utilized for this purpose.

Eighty four thermocouples were used in total. Sixty four of these were located on the discrete heat sources. Temperatures were also measured at the inlet, outlet, ambient, at several locations on the top and side walls of the insulation applied. The thermocouples on the heated section were inserted through holes drilled in the insulation, and were pushed into drilled cavities placed inside the copper blocks and soldered for rigidity. All thermocouples were separately calibrated. Signals from the thermocouples were collected, processed, stored and analyzed with a data acquisition system. This system consisted of two AXIOM AX5232 parallel-connected data acquisition cards located inside a PC computer. The whole process was controlled with a computer program developed specially for this experimental study.

It was observed that experimental conditions reach a steady-state condition after approximately 3–5 h. After conditions had been steady for some time and differences in temperatures between two intervals became negligible ($\Delta T < 0.1$ °C), all temperatures were collected, averaged and stored.

2.2. Processing of the experimental data

The amount of heat dissipation from each of the discrete heat sources in one row was very close to each other for all the experiments. Under this condition, experimental data were reduced in terms of a row-average Nusselt number for each of the bottom and the top heater row j as given below.

$$\overline{Nu}_{j\,\mathrm{bottom}} = \frac{Q_{\mathrm{c}_{j\,\mathrm{bottom}}} D_{\mathrm{h}}}{A_{\mathrm{s}_j}(\overline{T}_{\mathrm{s}_{j\,\mathrm{bottom}}} - T_{\mathrm{b}})k_{\mathrm{air}}} \tag{1}$$

$$\overline{Nu}_{j\,\mathrm{top}} = \frac{Q_{\mathrm{c}_{j\,\mathrm{top}}} D_{\mathrm{h}}}{A_{\mathrm{s}_j}(\overline{T}_{\mathrm{s}_{j\,\mathrm{top}}} - T_{\mathrm{b}})k_{\mathrm{air}}} \tag{2}$$

In these equations Q_{c_j} and A_{s_j} are total values for each row j of the top and bottom heaters. The hydraulic diameter D_{h} was used as the characteristic length as given below.

$$D_{\mathrm{h}} = \frac{4A_{\mathrm{c}}}{P} \tag{3}$$

Here A_{c} is the cross-sectional area and P is the perimeter of the channel. The bulk-mean temperature T_{b} was calculated from an energy balance applied to a control volume comprising one row of both top and bottom heaters together with non-heated sections. All thermo-physical properties were evaluated at this bulk-mean temperature. $\overline{T}_{\mathrm{s}}$ is the row-average heater temperature calculated from the thermocouple measurements. A_{s} is the total heater area in one row. Q_{c} is the corrected heat dissipation rate, which represents the heat transferred to the fluid directly by convection through the heater face. In the calculation of Q_{c} substrate conduction losses were taken into account as explained by Mahaney et al. [16]. Q_{c} was calculated from an energy balance and expressed for bottom and top heater row as given below.

$$Q_{\mathrm{c}_{j\,\mathrm{bottom}}} = Q_{\mathrm{tot}j\,\mathrm{bottom}} - Q_{\mathrm{rad}j\,\mathrm{bottom}} - Q_{\mathrm{cond}j\,\mathrm{bottom}} \tag{4}$$

and

$$Q_{\mathrm{c}_{j\,\mathrm{top}}} = Q_{\mathrm{tot}j\,\mathrm{top}} - Q_{\mathrm{rad}j\,\mathrm{top}} - Q_{\mathrm{cond}j\,\mathrm{top}} \tag{5}$$

In these calculations, first the total heat addition from resistance heaters was determined for each of bottom and top heater rows from

$$Q_{\mathrm{tot}_j} = 4\frac{V^2}{R} \tag{6}$$

where V is the voltage drop across the heater and R is the resistance of the heater. From this value Q_{c} was calculated by subtracting losses due to conduction and radiation. For bottom and top heaters, radiative heat transfer was also taken into account using the following equation:

$$Q_{\mathrm{rad\,bottom}(i,j)} = \sigma\varepsilon A_{\mathrm{s}} F(T^4_{\mathrm{s\,bottom}(i,j)} - \overline{T}^4_{\mathrm{b}}) \tag{7}$$

and

$$Q_{\mathrm{rad\,top}(i,j)} = \sigma\varepsilon A_{\mathrm{s}} F(T^4_{\mathrm{s\,top}(i,j)} - \overline{T}^4_{\mathrm{b}}) \tag{8}$$

where the view factor F between the heat source and its surroundings was taken to be unity (see e.g. [6,14,15,24,25]) and the surface emissivity was measured to be 0.3. Here, a single heat source was assumed to be surrounded by large surfaces at the bulk temperature of the fluid.

Here $\overline{T}_b$ was calculated from:

$$\overline{T}_b = \frac{T_{b_j} + T_{b_{j+1}}}{2} \tag{9}$$

where the arithmetic average of the bulk-mean fluid temperature for two adjacent rows is calculated.

Other dimensionless numbers affecting the heat transfer are

The Reynolds number:

$$Re_{D_h} = \frac{U_{in} D_h}{\nu_{air}} \tag{10}$$

The modified Grashof number:

$$Gr^*_{D_h} = \frac{g\beta \bar{q}_c D_h^4}{k_{air}\nu_{air}^2} \tag{11}$$

The modified Rayleigh number:

$$Ra^*_{D_h} = Gr^*_{D_h} Pr \tag{12}$$

The Richardson number:

$$Ri = \frac{Gr^*_{D_h}}{Re^2_{D_h}} \tag{13}$$

where $\bar{q}_c$ is the average convection heat flux for all the heaters.

In order to determine the reliability of the experimental results, an uncertainty analysis was conducted on all measured quantities as well as the quantities calculated from the measurement results. Uncertainties were estimated according to the standard procedures reported in the literature, see e.g. [26–30]. Overall, the uncertainty in the Nusselt number is around ±6% and for the Grashof number it is around ±4%, which is primarily due to uncertainties in the convective heat flux values. Uncertainty in the Reynolds number is around ±3%.

3. Results and discussion

Mixed convection heat transfer in a top and bottom heated horizontal channel with arrays of discrete heat sources has been investigated experimentally for aspect ratios of 2, 4 and 10. Experiments were conducted under various flow conditions. The values of parameters corresponding to these conditions are listed in Table 1.

The results of the present study are presented using the modified Grashof number Gr^* based on heat flux and the channel geometry (see Eq. 11). As a consequence of the above mentioned experimental conditions, the Richardson number was obtained between 0.51 and 367. For large Richardson numbers, the flow was assumed to be natural convection dominated.

In Fig. 2, typical row-average surface temperature distributions of top and bottom heaters are presented in the main flow direction for AR = 2, $Re = 1459$ and different Grashof numbers. The row-average surface temperatures of both top and bottom heaters increase with Grashof number. As can be seen from this figure, values of row-average surface temperatures of top heaters are greater than those of bottom heaters when natural convection effects become dominant at high values of Grashof numbers such as $Gr^* = 1.9 \times 10^9$. This can be attributed to the fact that top heaters are not affected much from the buoyancy-driven secondary flow. They are mainly affected by the forced convection due to the velocity in the main flow

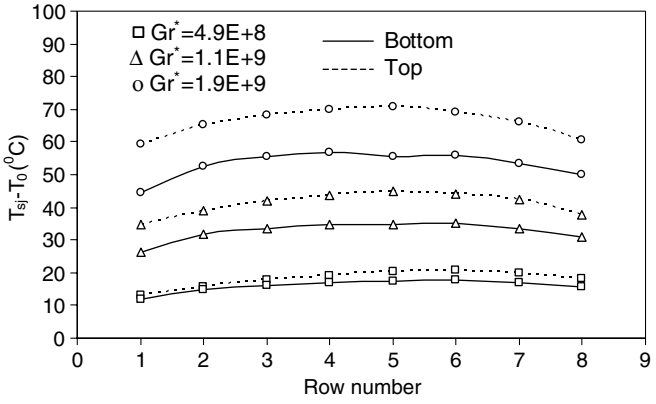

Fig. 2. Effect of Grashof number on row-average temperatures for AR = 2 and $Re = 1459$.

Table 1
Parametric conditions of the cases studied

AR	Re_{D_h}	$Gr^*_{D_h}$	AR	Re_{D_h}	$Gr^*_{D_h}$	AR	Re_{D_h}	$Gr^*_{D_h}$
2	380	4.9×10^8	4	825	6.2×10^7	10	937	2.8×10^6
2	380	1.1×10^9	4	825	1.4×10^8	10	937	6.4×10^6
2	380	1.9×10^9	4	825	2.5×10^8	10	937	1.1×10^7
2	792	4.9×10^8	4	1185	6.2×10^7	10	1421	2.8×10^6
2	792	1.1×10^9	4	1185	1.2×10^8	10	1421	6.4×10^6
2	792	1.9×10^9	4	1185	2.5×10^8	10	1421	1.1×10^7
2	1459	4.9×10^8	4	1459	1.4×10^8	10	1459	6.4×10^6
2	1459	1.1×10^9	4	1700	6.2×10^7	10	1872	2.8×10^6
2	1459	1.9×10^9	4	1700	1.2×10^8	10	1872	6.4×10^6
2	2446	4.9×10^8	4	1700	2.5×10^8	10	1872	1.1×10^7
2	2446	1.1×10^9	4	2025	6.2×10^7	10	2337	2.8×10^6
2	2446	1.9×10^9	4	2025	1.2×10^8	10	2337	6.4×10^6
			4	2052	2.5×10^8	10	2337	1.1×10^7

direction. Thus, the fluid motion near the top heaters is established at lower rates which cause the surface temperatures of top heaters to become higher than those of bottom heaters. As Grashof number decreases, however, effects of forced convection increase causing the surface temperatures of top and bottom heaters at the same row to approach each other as seen in Fig. 2 for the lowest value of Grashof number ($Gr^* = 4.9 \times 10^8$).

Fig. 3 presents row-average Nusselt number distributions of bottom and top heaters in the main flow direction with respect to row number for AR = 2, $Re = 1459$ and different Grashof numbers. For bottom heaters, Nusselt numbers decrease with the row number until the fourth row of heaters at values of Grashof numbers, $Gr^* = 1.9 \times 10^9$ and $Gr^* = 1.1 \times 10^9$. After the fourth row however, there is an increase in Nusselt number due to the effects of natural convection which becomes important by the onset of secondary flow after this row of heaters. With the decrease in Grashof number, natural convection effects become important at later rows of heaters and therefore, Nusselt numbers start increasing after sixth row for $Gr^* = 4.9 \times 10^8$. As can be seen from the same figure, for top heaters, there is no substantial change in Nusselt number until the fifth row for $Gr^* = 1.9 \times 10^9$ and 1.1×10^9. The increase in the row-average Nusselt number can be noticed for the sixth to eighth rows of top heaters. This increase can be explained by considering the buoyancy-induced secondary flow which is more effective at the last rows of top heaters. The magnitudes of velocities associated with the secondary flow are greater for these rows, thus, an increase in Nusselt number occur in the direction of main flow after the onset of natural convection. In the entrance region of the channel the Nusselt number variations show a forced convection entrance region characteristic for $Gr^* = 4.9 \times 10^8$ as also seen for all Grashof numbers of bottom heaters.

Fig. 4 presents row-average Nusselt number variations for AR = 2, $Gr^* = 1.1 \times 10^9$ and Reynolds numbers, $Re =$ 380, 792, 1459 and 2446. The place where the Nusselt number starts increasing shifts towards the first rows of

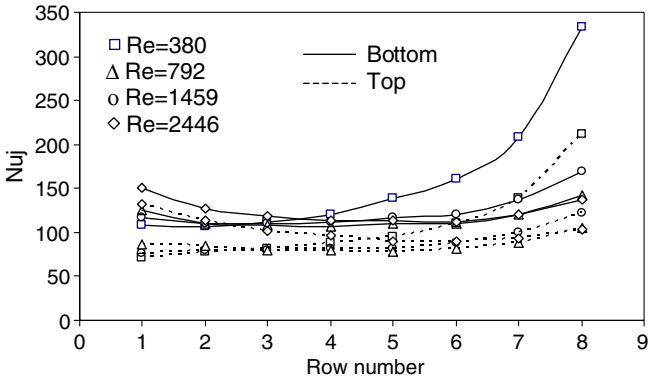

Fig. 4. Effect of Reynolds number on row-average Nusselt numbers for AR = 2 and $Gr^* = 1.1 \times 10^9$.

heaters with decrease in the Reynolds number for both bottom and top heaters. This is due to the fact that natural convection becomes more important at low values of Reynolds number.

The row-average surface temperature distributions in the main flow direction for the eight rows of bottom and top heaters are shown in Fig. 5 for AR = 4, $Re = 825$ and different Grashof numbers. As can be seen from Fig. 5 heater temperatures first increase in the main flow direction with the row number and then this increase stops at about the fourth row. After the sixth row, the temperatures start decreasing. For the top plate, however, the increase in temperature with the row number can continue until the seventh row. These graphics show clearly how the Grashof number affects the surface temperatures. Overall, increasing the Grashof number results in an increase of the heater temperatures. A comparison of surface temperatures of top heaters with those of bottom heaters shows that row-average surface temperatures at the top surface are bigger for a given Grashof number, especially for the highest Grashof number ($Gr^* = 2.5 \times 10^8$). This is due to the low velocity regions occurring near the top heaters.

Fig. 6 presents row-average Nusselt number distributions for AR = 4, $Re = 825$ and different Grashof numbers.

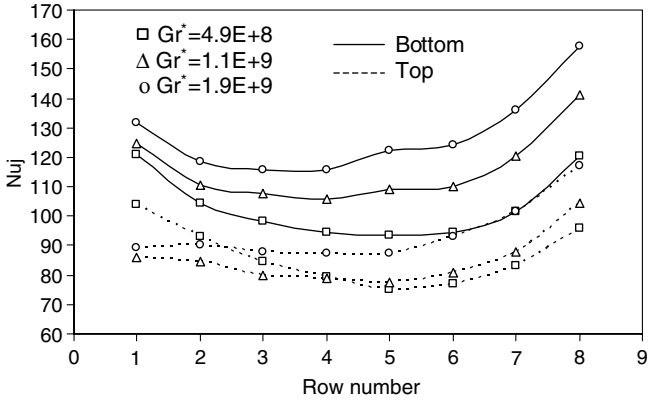

Fig. 3. Effect of Grashof number on row-average Nusselt numbers for AR = 2 and $Re = 1459$.

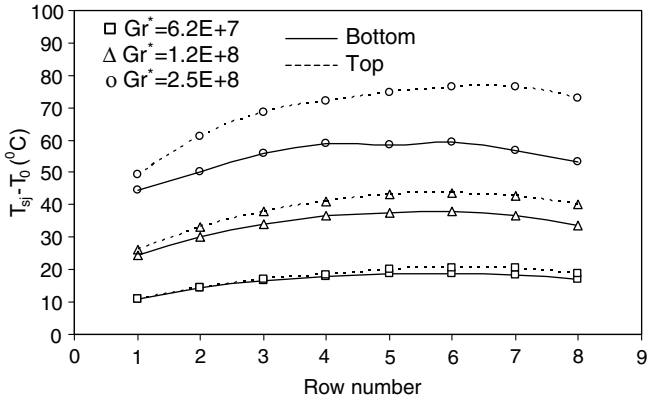

Fig. 5. Effect of Grashof number on the row-average temperatures for AR = 4 and $Re = 825$.

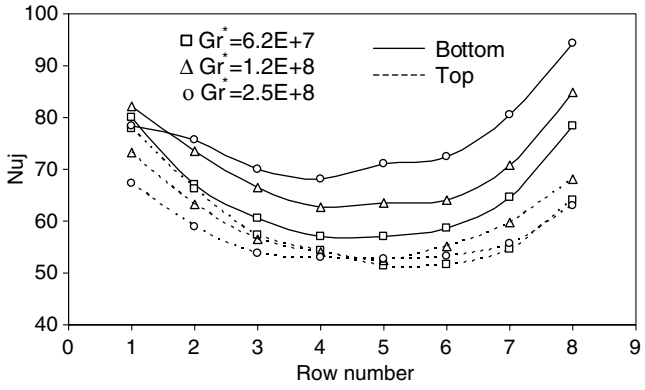

Fig. 6. Effect of Grashof number on row-average Nusselt numbers for AR = 4 and $Re = 825$.

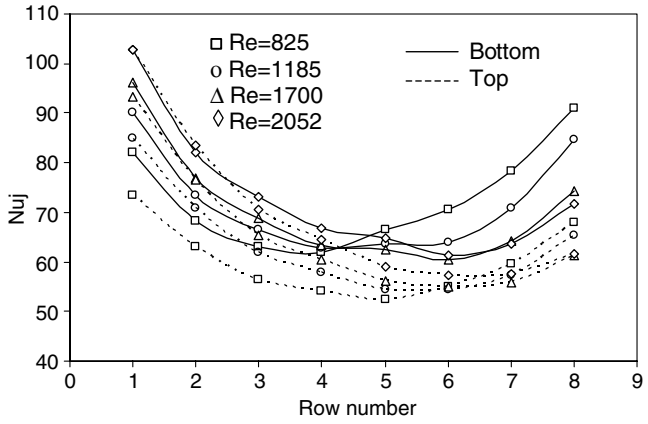

Fig. 7. Effect of Reynolds number on row-average Nusselt numbers for AR = 4 and $Gr^* = 1.4 \times 10^8$.

As can be seen from this figure, in the entrance region of the channel, the Nusselt number variations show a forced convection entrance region characteristic. After the onset of instability, however, at approximately the fourth row for the bottom plate, the buoyancy driven secondary flow inhibits the continuous drop in the local Nusselt number. This is a result of the buoyancy forces that become strong enough to destabilize the boundary layer. This effect is due to the decrease in the density of the fluid, which accelerates development of the secondary flow. Consequently, an increase in the Nusselt number is observed. The region after the start of the secondary flow conditions can be described as the mixed convection dominated region. Effects of changes in the Grashof number on the row-average Nusselt number are also shown in Fig. 6. It can be seen that Nusselt numbers increase with Grashof number for bottom heaters. For top heaters, however, they decrease with the Grashof number for the fully developed forced convection dominated region until the fifth row of heaters in the main flow direction. After the fifth row, the heat transfer is enhanced due to the buoyancy forces and the flow includes cross-stream velocities which cause the rising of hot fluid from the bottom heat sources toward the top ones, and therefore the variation of Nusselt numbers with the Grashof number shows a peculiar behavior after this row.

Row-average Nusselt number distributions are shown in Fig. 7 for different Reynolds numbers. These distributions are for the Grashof number of $Gr^* = 1.4 \times 10^8$ and AR = 4. The first three rows for both bottom and top heaters show clear differences at different Reynolds numbers, where large Reynolds numbers produce larger Nusselt numbers at the beginning of the heated section. These differences diminish at row numbers 4 and 5 for the bottom heaters and 6 and 7 for the top ones. In this region, the reduction in the Nusselt number due to forced convection effects is balanced by an increase due to the buoyancy-driven secondary flow. Starting with row number 6 for the bottom heaters, differences in Nusselt numbers for different Reynolds numbers become visible again. However, this time the results in terms of the Nusselt values are reversed. Similar behavior of the Nusselt numbers is shown after the seventh row for top heaters. In the entrance region of the channel, the Nusselt number variations show a forced convection thermal entry region characteristic. However, after the onset of instability at the fifth or sixth rows the buoyancy driven secondary flow inhibits the continuous drop in the local Nusselt number for both bottom and top heaters. After the sixth row a clear increase in the heat transfer is observed due to the above explained effects. With the decrease in Reynolds number, the place where the development of the secondary flow occurs moves towards the first row of heaters ($Re = 825$). At the largest Reynolds number ($Re = 2052$), the heaters are under the effect of forced convection dominated flow. Therefore Nusselt number decreases with the row number except for the last two rows, where the effects of buoyancy induced secondary flow become important.

The row-average surface temperature distributions of the heaters in the main flow direction for the eight rows of bottom and top heaters are shown in Fig. 8 for AR = 10, $Re = 937$ and for different Grashof numbers. Heater surface temperatures continuously increase in the main flow direction with the row number. These graphics

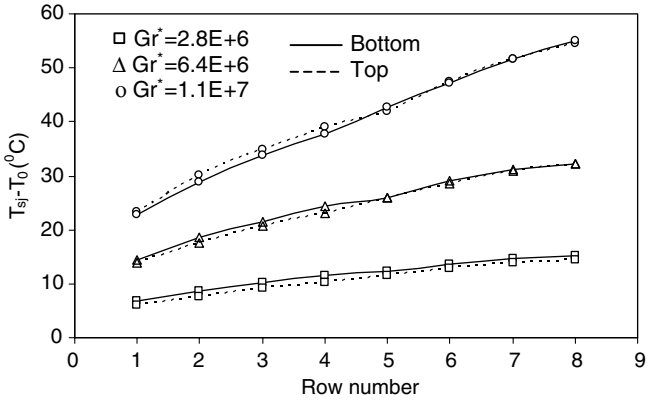

Fig. 8. Effect of Grashof number on row-average temperatures for AR = 10 and $Re = 937$.

also show clearly how the Grashof number affects the heater surface temperatures. The larger the Grashof number, the higher the surface temperatures as for the cases of AR = 2 and AR = 4 presented in Figs. 2 and 5, respectively. As can be seen from Fig. 8, however, surface temperatures increase almost linearly with the row number, which present a different behavior compared to the previous cases. For the case of Fig. 8, both the bottom and the top heaters are affected mainly by forced convection flow and the boundary layer associated with bottom and top do completely influence each other. Under these conditions, effects of buoyancy driven flow are much smaller and almost vanish.

Fig. 9 presents row-average Nusselt number distributions for bottom and top heaters for AR = 10, $Re = 937$ and different Grashof numbers. Variations shown in this figure are different from the distributions of Figs. 3 and 6 which present variations in Nusselt number for AR = 2 at $Re = 1459$ and AR = 4 at $Re = 825$, respectively. Forced convective flow is more dominant for both the bottom and the top heaters at all Grashof numbers in this case. Therefore, Nusselt number can continuously decrease with the row number in the flow direction.

Effect of the Reynolds number on the row-average Nusselt numbers are shown in Fig. 10 for AR = 10 and $Gr^* = 6.4 \times 10^6$. Variations shown in this figure show typical forced convective flow characteristics for all Reynolds numbers. These variations with Reynolds number are similar to the distributions of Fig. 9 which show the effects of Grashof number. But they are quite different from the distributions of Figs. 4 and 7 which involve the effects of buoyancy driven secondary flow. This is due to the low values of Richardson number ($Ri = 0.51$–12.52) associated for the case of AR = 10 that causes smaller effects of free convection heat transfer. In order to see this more clearly Fig. 11 was drawn which shows effects of aspect ratio on Nusselt number distributions. As can be seen from this figure, the experiments were performed at additional Reynolds numbers for better comparison. The free convection effects change according to the row number and aspect ratio. The buoyancy driven secondary flow has positive effects on the Nusselt number for AR = 2 at $Gr^* = 1.1 \times 10^9$ and AR = 4 at $Gr^* = 1.4 \times 10^8$. For AR = 10 at $Gr^* = 6.4 \times 10^6$, however, forced-convection dominated flow occurs, and therefore no differences between distributions of Nusselt number for bottom and top heaters occur as can be seen from Fig. 11. The highest values of *Nu* numbers are obtained for the case of AR = 2 for which the cross-sectional area is $A_c = 0.02\ m^2$. As A_c is decreased to $0.01\ m^2$ and $0.004\ m^2$ for the cases of AR = 4 and AR = 10, respectively, row-average *Nu* numbers decrease accordingly. This is due to the fact that the decrease in area means smaller values of hydraulic diameter D_h, which results in higher main flow velocities at the constant value of Reynolds number ($Re = 1459$). The modified Grashof number $Gr^*_{D_h}$, however, decreases with D_h. Thus, the increase in AR causes an increase in the main flow velocity at lower Grashof numbers that decreases the positive effects of the buoyancy driven secondary flow on the *Nu* number.

The influence of buoyancy effects on the row average Nusselt number are also shown in Fig. 12 at different Rayleigh numbers. Figs. 12(a)–(d) present variation of Nusselt number with Reynolds number for bottom and top heaters at $j = 1$, 3, 5 and 7 rows, respectively. As can be seen from

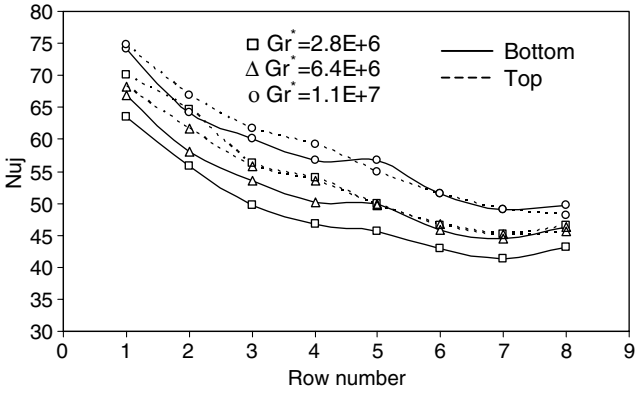

Fig. 9. Effect of Grashof number on row-average Nusselt numbers for AR = 10 and $Re = 937$.

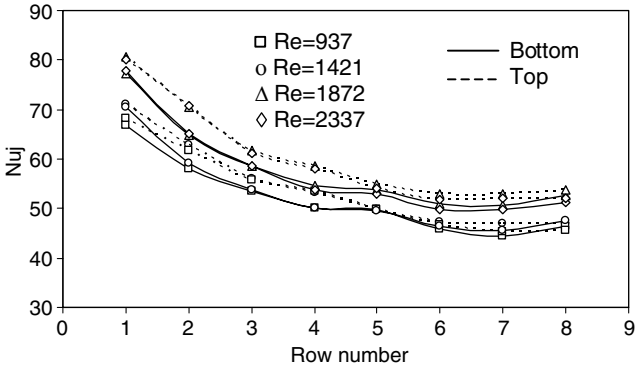

Fig. 10. Effect of Reynolds number on row-average Nusselt numbers for AR = 10 and $Gr^* = 6.4 \times 10^6$.

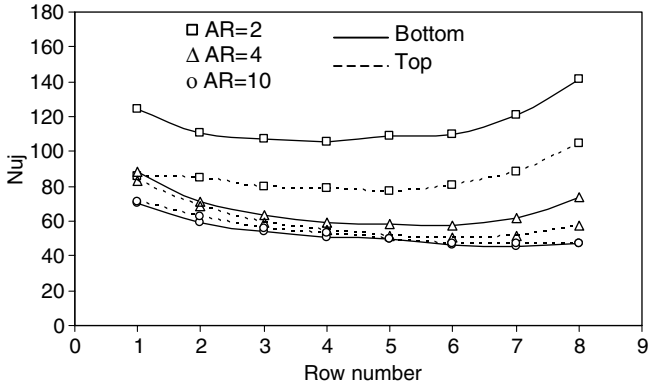

Fig. 11. Effect of aspect ratio on row-average Nusselt numbers for $Re = 1459$.

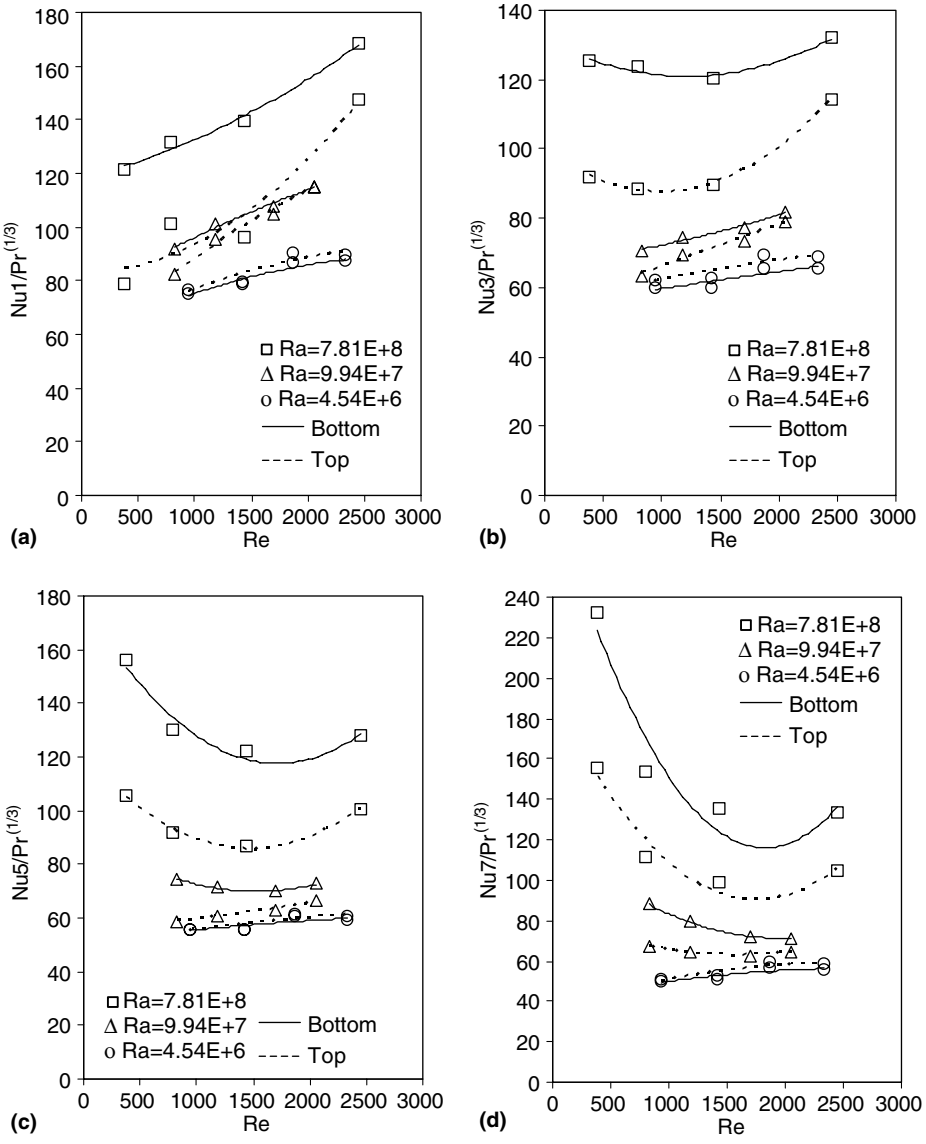

Fig. 12. Effects of Rayleigh and Reynolds numbers on row-average Nusselt number of bottom and top heaters with respect to row number: (a) first row, (b) third row, (c) fifth row, (d) seventh row.

these figures, row-average Nusselt numbers take greater values at high Rayleigh numbers. The variation of Nusselt number with Rayleigh number, here, also shows the effect of aspect ratio, AR, since $Ra = 7.81 \times 10^8$, 9.94×10^7 and 4.54×10^6 correspond to AR = 2, 4 and 10, respectively. At high Rayleigh numbers or at low values of aspect ratios, the effects of buoyancy-driven secondary flow on Nusselt number becomes more important. This agrees with the results of the discussion in Fig. 11. The variation of row-average Nusselt number with the row number shows that Nusselt number increases with Reynolds number at row 1, but it becomes independent of Reynolds number below a certain limit for other rows, suggesting that heat transfer is dominated by natural convection under these conditions. The significant heat transfer enhancement associated with the secondary flow causes the Nusselt number at row 7 to exceed those at rows 3 and 5 for Reynolds numbers below about 800. Nusselt numbers for top heaters take smaller values than those of bottom heaters at the same row and Reynolds number. This is due to the reasons discussed previously. As also seen from Fig. 12, transition to turbulence may occur at a certain value of Reynolds number where a sudden increase in the Nusselt number is noticed (for $Re > 2000$).

4. Conclusions

The problem of mixed convection heat transfer in a horizontal channel with heated top and bottom discrete heat sources has been studied experimentally. Experimental results for $2 \times (8 \times 4)$ flush mounted heat sources subjected to uniform heat flux, on both the top and bottom walls of the channel have been presented for different aspect ratios and ranges of Grashof and Reynolds number.

For small values of aspect ratios such as $AR = 2$, the effects of free convection become more important. Especially, at high values of Grashof numbers, the effects of buoyancy-driven secondary flow increase with the row number for both bottom and top heaters. The fluid motion near the top heaters, however, is established at lower rates and therefore these heaters have higher temperatures compared to the bottom ones. The variations of row average Nusselt number with Reynolds and Grashof numbers exhibit a relative minimum for the aspect ratio of $AR = 4$, suggesting that, due to buoyancy induced flow, heat transfer may be enhanced by reducing the flow rate at high heat dissipation rates. This is not the case, however, for high aspect ratios such as $AR = 10$. For this aspect ratio, a relative minimum value of row-average Nusselt number could not be seen for the ranges of Reynolds number and Grashof numbers considered in this study.

Changes in Gr^* and Re numbers affect significantly the buoyancy-driven secondary flow, the onset of instability, and the resulting heat transfer enhancement above the forced convection limit for the aspect ratio $AR = 4$. As the Reynolds number is decreased and/or the Grashof number increased, heat transfer enhancement is obtained due to development of buoyancy induced secondary flow. Thermal instabilities were either delayed or disappeared completely for large Reynolds numbers. Nusselt number variations for the first rows show a forced convection thermal entry region characteristic. However, after the onset of instability the buoyancy driven secondary flow changes the local Nusselt number variation. This is a result of the buoyancy forces that become strong enough to destabilize the boundary layer, and development of a secondary flow is started. As a consequence, an increase in the Nusselt number is observed. The region after the start of the secondary flow conditions can be described as the mixed convection dominated region.

For the conditions of this study, top heaters are more affected by the forced convection flow. Although some important effects of the secondary flow can be seen for small Reynolds numbers and low aspect ratios, these effects vanish for high values of aspect ratios.

These results suggest several guidelines for the thermal design of electronic packages. A device placed on the top wall will realize temperatures much higher than that of the lower wall. When dealing with high power densities in horizontal channel flow, the greater power dissipaters should be placed along the lower wall. In addition to this, electronic components with the greatest power dissipation should be placed on the first and last two rows at the bottom. While, low power dissipation components should always be placed around the middle section. This, however, is only valid for environments correctly arranged so that mixed convection heat transfer conditions are obtained for the electronic packaging. Moreover, the fact that the heat transfer enhancement is largest for low Reynolds numbers, suggests that heat transfer may be enhanced due to buoyancy-induced flow by reducing the flow rate and hence the ventilation power requirements.

Acknowledgements

Financial support of this study by the research fund of the Gazi University under Grant No. MMF06/2001-16 is gratefully acknowledged.

References

[1] K.J. Kennedy, A. Zebib, Combined free and forced convection between horizontal parallel planes: some case studies, Int. J. Heat Mass Transfer 26 (1983) 471–474.
[2] F.P. Incropera, J.S. Kerby, D.F. Moffatt, S. Ramadhyani, Convection heat transfer from discrete heat sources in a rectangular channel, Int. J. Heat Mass Transfer 29 (1986) 1051–1058.
[3] G.P. Peterson, A. Ortega, Thermal control of electronic equipment and devices, Adv. Heat Transfer 20 (1990) 181–314.
[4] T.J. Heindel, F.P. Incropera, S. Ramadhyani, Conjugate natural convection from an array of discrete heat sources: Part 1—Two and three dimensional model validation, Int. J. Heat Fluid Flow 16 (1995) 501–510.
[5] M. Choi, K. Cho, Effect of the aspect ratio of rectangular channels on the heat transfer and hydrodynamics of paraffin slurry flow, Int. J. Heat Mass Transfer 44 (2001) 55–61.
[6] A.B McEntire, B.W. Webb, Local forced convective heat transfer from protruding and flush-mounted two-dimensional discrete heat sources, Int. J. Heat Mass Transfer 33 (1990) 1521–1533.
[7] S.V. Garimella, P.A. Eibeck, Heat transfer characteristics of an array of protruding elements in single phase forced convection, Int. J. Heat Mass Transfer 33 (1990) 2659–2669.
[8] H. Turkoglu, N. Yucel, Mixed convection in vertical channels with a discrete heat source, Heat Mass Transfer 30 (1995) 159–166.
[9] M. Fuji, S. Gima, T. Tomimura, X. Zhang, Natural convection to air from an array of vertical parallel plates with discrete and protruding heat sources, Int. J. Heat Fluid Flow 17 (1996) 483–490.
[10] C.P. Tso, G.P. Xu, K.W. Tou, An experimental study on forced convection heat transfer from flush-mounted discrete heat sources, J. Heat Transfer 121 (1999) 326–332.
[11] Y.L. Tsay, Transient conjugate mixed-convective heat transfer in a vertical plate channel with one wall heated discretely, Heat Mass Transfer 35 (1999) 391–400.
[12] C. Yucel, M. Hasnaoui, L. Robillard, E. Bilgen, Mixed convection heat transfer in open ended inclined channels with discrete isothermal heating, Numer. Heat Transfer A 24 (1993) 109–126.
[13] C.Y. Choi, A. Ortega, Mixed convection in an inclined channel with a discrete heat source, Int. J. Heat Mass Transfer 36 (1993) 3119–3134.
[14] C.W. Leung, H.J. Kang, S.D. Probert, Horizontal simulated printed-circuit board assembly in fully-developed laminar-flow convection, Appl. Energy 56 (1997) 71–91.
[15] C.W. Leung, H.J. Kang, Convective heat transfer from simulated air-cooled printed-circuit board assembly on horizontal or vertical orientation, Int. Commun. Heat Mass Transfer 25 (1998) 67–80.
[16] H.V. Mahaney, F.P. Incropera, S. Ramadhyani, Comparison of predicted and measured mixed convection heat transfer from an array of discrete heat sources in horizontal rectangular channel, Int. J. Heat Mass Transfer 33 (1990) 1233–1245.
[17] J. Hacohen, T.W. Chiu, A.A. Wragg, Forced and free convective heat transfer coefficients for a model printed circuit board channel geometry, Exp. Thermal Fluid Sci. 10 (1995) 327–334.
[18] J.J. Hwang, Conjugate heat transfer for developing flow over multiple discrete thermal sources flush-mounted on the wall, J. Heat Transfer 120 (1998) 510–514.
[19] H.V. Mahaney, S. Ramadhyani, F.P. Incropera, Numerical simulation of three-dimensional mixed convection heat transfer from an

array of discrete heat sources in a horizontal rectangular duct, Numer. Heat Transfer 16 (1989) 267–286.
[20] A. Ozsunar, S. Baskaya, M. Sivrioglu, Numerical analysis of Grashof number, Reynolds number and inclination effects on mixed convection heat transfer in rectangular channels, Int. Commun. Heat Mass Transfer 28 (2001) 985–994.
[21] A. Ozsunar, S. Baskaya, M. Sivrioglu, Experimental investigation of mixed convection heat transfer in a horizontal and inclined rectangular channel, Heat Mass Transfer 38 (2002) 271–278.
[22] A. Dogan, M. Sivrioglu, S. Baskaya, Experimental investigation of mixed convection heat transfer in a rectangular channel with discrete heat sources at the top and at the bottom, Int. Commun. Heat Mass Transfer 32 (2005) 1244–1252.
[23] A. Dogan, Investigation of mixed convection heat transfer from a rectangular cross-section channel with discrete heat sources at the top and at the bottom, PhD thesis, Gazi University, Ankara, Turkey, 2003.
[24] C.G. Rao, C. Balaji, S.P. Venkateshan, Effect of surface radiation on conjugate mixed convection in a vertical channel with a discrete heat source in a each wall, Int. J. Heat Mass Transfer 45 (2002) 3331–3347.
[25] E. Kchoc, M. Davics, D. Newport, Mixed convection cooling of horizontally mounted printed circuit board, IEEE Trans. Comp. Packag. Technol. 26 (2003) 126–133.
[26] R.J. Moffat, Contributions to the theory of single-sample uncertainty analysis, J. Fluids Eng. 104 (1982) 250–260.
[27] R.J. Moffat, Using uncertainty analysis in the planning of an experiment, J. Fluids Eng. 107 (1985) 173–178.
[28] R.B. Abernethy, R.P. Benedict, R.B. Dowdell, ASME measurement uncertainty, J. Fluids Eng. 107 (1985) 161–164.
[29] S.J. Kline, The purposes of uncertainty analysis, J. Fluids Eng. 107 (1985) 153–160.
[30] R.E. Smith Jr., S. Wehofer, From measurement uncertainty to measurement communications, credibility, and cost control in propulsion ground test facilities, J. Fluids Eng. 107 (1985) 165–172.